Ab Initio Studies on the Dynamical Properties of the Reaction $NH(X^3\Sigma^-) + H \rightarrow N(^4S) + H_2$

Zhen-Feng Xu, De-Cai Fang, and Xiao-Yuan Fu*

Department of Chemistry, Beijing Normal University, Beijing 100875, People's Republic of China

Received: December 18, 1996; In Final Form: April 8, 1997[⊗]

The geometries of the reactant, product, and transition state of the titled reaction were optimized at the UHF, UMP2, and UMP4 levels with the double- and triple-ζ basis sets as well as polarization functions using the energy gradient method. The potential barrier for this reaction was calculated to be 1.68 kcal/mol at the MP-SAC4/6-311G** level. The intrinsic reaction coordinate (IRC) was traced at the UMP2/6-311G** level, and the energy profile along the IRC was refined with the subsequent MP-SAC4/6-311G** calculations. The calculated rate constants at the MP-SAC4/6-311G** level are in good agreement with the experimental values in the temperature range 2000−3000 K.

Introduction

The pyrolysis of ammonia (NH_3) includes a series of radical reactions. The ground-state hydrogen abstraction reaction

$$NH(X^3\Sigma^-) + H \rightarrow N(^4S) + H_2$$

is the important one among these radical reactions. It plays a significant role not only in the decay of imidogen (NH) in the pyrolysis of ammonia[1,2] but also in the gas-phase combustion reactions of nitrogen compounds.[3] Owing to the complexity of the overall reactions, it is difficult to extract experimentally reliable rate constants for the elementary reactions from the kinetic studies of ammonia pyrolysis. The rate constant can only be obtained indirectly. In 1981, Morley[4] measured a value for the reaction rate constant over the temperature range 1790−2200 K. In 1990, Davidson and Hanson[5] gave the reverse reaction rate constant by using N-atom ARAS measurements from 1950 to 2850 K. Their rate constant is expressed as $1.6 \times 10^{14} \exp(-25140/RT)$ ($cm^3\ mol^{-1}\ s^{-1}$), and its equivalent forward rate constant formula can be written as $3.2 \times 10^{13} \exp(-325/RT)$ ($cm^3\ mol^{-1}\ s^{-1}$). The result is in good agreement with the Morley's. Early in 1963, Mayer and Schieler[6] estimated the activation energy and rate constant by using the Johnston and Parr[7] method. No further studies have been found since then.

Direct dynamical calculations based on variational transition state theory (VTST) is a practical methodology for polyatomic reactions.[8−11] It describes a chemical reaction by using ab initio electronic structure information only in the region of configuration space along the reaction path. Recently, we have studied the dynamical properties of the ground-state reaction $NH(X^3\Sigma^-) + H \rightarrow N(^4S) + H_2$, and the calculated rate constants are very close to the experimental results.[12]

In the present paper, we use the direct dynamical method for the hydrogen abstraction reaction $NH(X^3\Sigma^-) + H \rightarrow N(^4S) + H_2$ for the temperature range 2000−3000 K. The information about the electronic energy and energy derivatives was calculated along the intrinsic reaction coordinate (IRC).[13] In the second section, the theoretical methods and calculation details were given. The third section represents the location of the stationary points and minimum energy path (MEP). In light of the reaction-path Hamiltonian,[14] the reaction-path curvature and the coupling constants between the IRC and the normal vibrational modes perpendicular to the IRC were discussed. At the end of the third section, the calculated reaction rate constants using the improved potential energy curves were presented.

Calculational Methods

In this work, standard ab initio molecular orbital calculations were carried out with the GAUSSIAN 92 program[15] for the stationary points on the reaction path of the title reaction. The geometries of the reactant (NH), product (H_2), and transition state (TS) were optimized by using unrestricted Hartree−Fock (UHF) theory,[16] spin-unrestricted Møller−Plesset perturbation (UMP) theory,[17,18] and spin-unrestricted quadratic configuration interaction with all single and double substitutions (UQCISD(T)) theory,[19] respectively. The second-order Møller−Plesset perturbation (UMP2) calculations include full electron correlation. And for the fourth-order Møller−Plesset perturbation (UMP4) and UQCISD(T) calculations, the frozen-core approximation was used. Furthermore, we have scaled all correlation (SAC) energy in the UMP4/6-311G** calculation to yield an improved calculation of the barrier height at the UMP2/6-311G** optimized geometries, which is called the MP-SAC4//MP2 level.[20] In the MP-SAC4//MP2 calculation, the total electronic energy is written as[20]

$$E_{\mathrm{MP-SAC4//MP2}} = E_{\mathrm{HF}} + (E_{\mathrm{MP4}} - E_{\mathrm{HF}})/f_4$$

where f_4 is a scaling factor that is assumed to be independent of geometry for a given system.

The tracing of IRC at the UMP2/6-311G** level with a step size of 0.02 $amu^{1/2}$ bohr was performed. At some points along the intrinsic reaction coordinate (IRC), we computed the matrix of force constants, the harmonic vibrational frequencies, and the corresponding normal-mode vectors for the $3N - 7$ degrees of freedom transverse to the reaction path. Because the shape of the potential energy curve is an important factor affecting the rate constant, several points near the TS along the UMP2 potential profile was refined at the UMP4, UQCISD(T), and MP-SAC4 levels with the same basis set.

The generalized transition state theory rate constant k^{GT} for temperature T and dividing surface at s can be expressed as[9]

$$k^{\mathrm{GT}}(T,s) = \frac{\sigma Q^{\mathrm{GT}}(t,s)}{\beta h \phi^{\mathrm{R}}(T)} \exp(-\beta V_{\mathrm{MEP}}(s))$$

[⊗] Abstract published in *Advance ACS Abstracts,* May 1, 1997.

S1089-5639(97)00031-5 CCC: $14.00

In this equation, s is the location of the generalized transition state on the IRC; σ is the symmetry factor accounting for the possibility of two or more symmetry-related reaction paths; β equals $(k_B T)^{-1}$ where k_B is Boltzmann's constant, h is Plank's constant; $\phi^R(T)$ is the reactant's partition function per unit volume, excluding symmetry numbers for rotation; $V_{MEP}(s)$ is the classical energy along the MEP overall zero of energy at the reactant; $Q^{GT}(T,s)$ is the partition function of a generalized transition state at s with a local zero of energy at $V_{MEP}(s)$ and with all rotational symmetry numbers set to unity. For $s = 0$, this equation becomes the expression of conventional transition-state theory.

According to canonical variational theory (CVT), the rate constant at fixed temperature (T) is obtained by minimizing k^{GT} with respect to the dividing surface at s, that is,[9]

$$k^{CVT}(T) = \min_s k^{GT}(T,s)$$

For the tunneling effect correction, a semiclassical transmission coefficient $\kappa^{CVT/MEPSAG}$ has been used in which the SAG represents a semiclassical adiabatic ground-state method. Therefore, the variational transition-state rate constant becomes[9]

$$k^{CVT/MEPSAG}(T) = \kappa^{CVT/MEPSAG}(T) k^{CVT}(T)$$

The $\kappa^{CVT/SAG}(T)$ may be expressed as

$$\kappa^{CVT/MEPSAG}(T) = \beta \exp(\beta V_a^G(s_*^{CVT}(T))) \int_0^\infty P^{SAG}(E) \exp(-\beta E)\, dE$$

Here, E is the total energy of the system relative to reactants, $P^{SAG}(E)$ is the one-dimensional transmission probability that corresponds to passing through the adiabatic ground-state potential energy curve $V_a^G(s)$; s_*^{CVT} is the temperature-dependent value of s at which k^{GT} has a minimum, i.e., location of the CVT transition state, $V_a^G(s)$ is the vibrationally adiabatic ground-state potential curve defined by $V_a^G(s) = V_{MEP}(s) + \epsilon_{int}^G(s)$, where $\epsilon_{int}^G(s)$ denotes the zero-point energy in vibrational modes transverse to the IRC.

To further consider the effect of the curvature of the reaction path, $\kappa^{CVT/MEPSAG}(T)$ is corrected by a small curvature (SC) approximation, which uses an effective mass for reaction coordinate motion,[9] and then is expressed as $\kappa^{CVT/SCSAG}(T)$. Therefore, the variational transition-state rate constant is as follows:

$$k^{CVT/SCSAG}(T) = \kappa^{CVT/SCSAG}(T) k^{CVT}(T)$$

The POLYRATE program[21] was employed in the calculations for the projection of the force constant matrix, coupling constants, and reaction rate constants.

All the calculations were carried out using the above-mentioned computer programs on a DEC-workstation 5000/133 computer in the Chemistry Department of Beijing Normal University.

Results and Discussion

A. Stationary Points. The optimized geometric parameters and vibrational frequencies of NH and H_2 optimized at various levels of theory are listed in Table 1. The polarization functions and electron-correlated energy are very important. For the reactant NH and product H_2, the bond lengths at the UMP2/6-311G** level are close to the experimental values and comparable to that at both the UMP4/6-311G** and the UQCISD(T)/6-311G** levels. However, the harmonic vibrational frequencies of NH and H_2 are about 3% greater than the experimental ones.

TABLE 1: Geometric Parameters and Frequencies of NH and H_2

	NH ($X^3\Sigma^-$)		H_2	
	R_{N-H} (Å)	ω (cm^{-1})	R_{H-H} (Å)	ω (cm^{-1})
UHF/6-31G	1.032	3372	0.730	4640
UHF/6-31G**	1.024	3514	0.733	4634
UHF/6-311G**	1.023	3501	0.736	4594
UMP2/6-311G**	1.034	3392	0.738	4534
UMP4/6-311G**	1.042	3295	0.742	4454
expt[21]	1.036	3282	0.741	4401

TABLE 2: Geometric Parameters and Frequencies of Linear Transition State $H_{(3)}—H_{(2)}—N_{(1)}$ ($^4\Sigma$)

	R_{12} (Å)	R_{23} (Å)	frequency (cm^{-1})			
			$\omega_1(\sigma)$	$\omega_2(\pi)$	$\omega_3(\pi)$	$\omega_4(\sigma)$
UHF/6-31G	1.138	1.203	i2084	766	766	1319
UHF/6-31G**	1.154	1.112	i2459	806	806	1354
UHF/6-311G**	1.154	1.103	i2450	797	797	1352
UMP2/6-311G**	1.130	1.103	i1748	824	824	1592
UMP4/6-311G**	1.111	1.190	i1311	574	602	1773

Table 2 lists the geometric parameters and frequencies of the linear transition state optimized at the UHF and UMPn levels. From this table, it can be seen that there are basically the same effects of basis set for the transition state as that for reactant and product. We also found that the imaginary vibrational frequencies at UMP2 and UMP4 levels are about 700 and 1100 cm^{-1} less than those at the UHF level, respectively. And the frequencies of the bound vibrational mode 4 at the UMP2 and UMP4 levels are about 240 and 420 cm^{-1} greater than those at the UHF level, respectively. This shows the electron correlation is obvious for the reaction process. Therefore, the reaction path properties were investigated at the UMP2 level.

To illustrate the feasibility of an unrestricted Hartree−Fock single-configuration reference state, a multiconfiguration self-consistent field (MCSCF) calculation was carried out to optimize the transition state. A complete active space involving five electrons and six orbitals is employed with the 6-311G** basis set. The result shows that the coefficient of the ground-state configuration is 0.982 and those of other configurations are all about 0.1 or less. Thus, a single ground-state determinant can afford a sufficiently accurate description of this reaction.

In Table 3, we summarized a variety of results for the total energies of reactants, products, and transition state, as well as the potential barrier height (ΔE) and the heat of reaction (ΔH). This table reveals that the energy of the reaction system strongly depends on the electronic correlation and basis set used. For this exothermic hydrogen abstraction reaction, the heat of reaction is well established experimentally as −24.34 kcal/mol.[5] The deviation of the heat of reaction between the calculation value at the UHF/6-31G level and the experimental one is 18.18 kcal/mol. Upon the addition of the polarization functions, it falls to 9.14 kcal/mol. Furthermore, with the electronic correlation added, the deviation is within about 6 kcal/mol. At the MP-SAC4 level, the heat of reaction is −28.59 kcal/mol and very close to the experimental value. For the activation energy of the reaction, there are two experimental estimated values: 0.325 kcal/mol determined recently[5] and 1.5 kcal/mol determined earlier.[6] It is obvious that the potential barriers calculated at the UHF level are overestimated. After addition of electronic correlation, the reaction barrier height drops greatly to 5.28 kcal/mol at the UMP2 level and 3.07 kcal/mol at the UMP4 level, respectively. Single-point calculations at the UQCISD(T) and MP-SAC4 levels give the lowest values of the reaction barrier that are closest to the experimental one.

TABLE 3: Total Energies, Potential Barrier, and Heat of Reaction

	total energies (au)				
	reactants		TS	products	
	NH	H	N−H−H	N	H_2
	Optimized				
UHF/6-31G	−54.942 94	−0.498 23	−55.430 94	−54.385 01	−1.126 83
UHF/6-31G**	−54.962 64	−0.498 23	−55.445 69	−54.385 44	−1.131 33
UHF/6-311G**	−54.976 06	−0.499 81	−55.460 91	−54.397 98	−1.132 49
UMP2/6-311G**	−55.106 45	−0.499 81	−55.597 50	−54.492 84	−1.160 27
UMP4/6-311G**	−55.107 77	−0.499 81	−55.601 90	−54.490 89	−1.167 74
	Single-Point Calculations at UMP2/6-311G** Geometry				
UMP4/6-311G**	−55.107 74	−0.499 81	−55.602 28	−54.490 89	−1.167 73
UQCISD(T)/6-311G**	−55.109 17	−0.499 81	−55.605 54	−54.491 42	−1.168 32
MP-SAC4/6-311G**	−55.138 65	−0.499 81	−55.635 46	−54.512 69	−1.173 95

	potential barrier[a] (kcal/mol)		heat of reaction[a] (kcal/mol)	
	ΔE	ΔE_{ZPE}	ΔH	ΔH_{ZPE}
	Optimized			
UHF/6-31G	6.42	5.68	−44.34	−42.52
UHF/6-31G**	9.52	8.74	−35.08	−33.48
UHF/6-311G**	9.38	8.59	−34.26	−32.7
UMP2/6-311G**	5.48	5.28	−29.40	−27.76
UMP4/6-311G**	3.56	3.07	−31.68	−30.02
	Single-Point Calculations at UMP2/6-311G** Geometry			
UMP4/6-311G**	3.31	3.11	−32.05	−30.41
UQCISD(T)/6-311G**	2.16	1.96	−31.85	−30.21
MP-SAC4/6-311G**	1.88	1.68	−30.23	−28.59
expt[5]	0.325		−24.34	
expt[6]	1.5		−20.1	

[a] ΔE_{ZPE} and ΔH_{ZPE} represent the results corrected by the zero-point vibration energy.

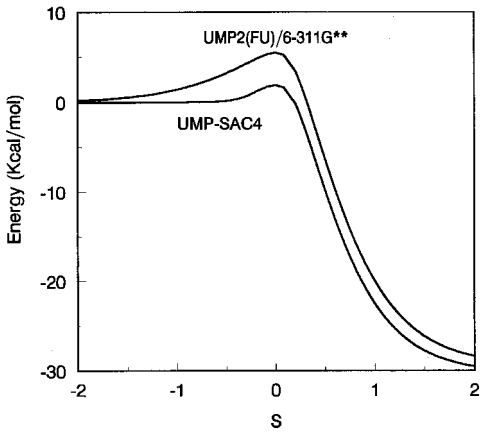

Figure 1. Profile of relative energy along the IRC as a function of s amu$^{1/2}$ bohr.

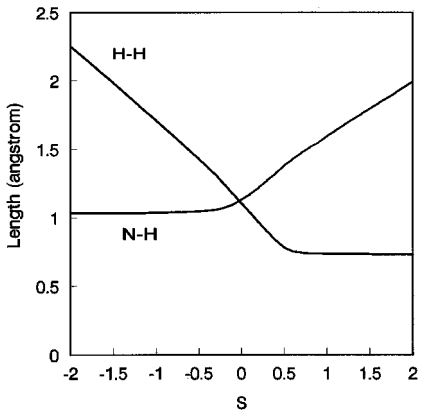

Figure 2. Changes of main geometric parameters along the IRC as a function of s amu$^{1/2}$ bohr.

Therefore, we assume that the barrier at MP-SAC4 level, 1.68 kcal/mol, is the best theoretical value.

B. Reaction-Path Dynamical Properties. According to the intrinsic reaction coordination (IRC) theory, we used the UMP2/6-311G** level with a step size of 0.02 amu$^{1/2}$ bohr to trace the minimum energy path of the reaction. The energy profile was further refined with the UQCISD(T)/6-311G** and MP-SAC4/6-311G** methods. Figure 1 shows the potential energy curves (V_{MEP}) along the IRC. It can be seen that the potential energy curves are very steep after the transition state. Figure 2 describes the geometrical changes along the IRC. It appears that the distance H−H shortens linearly before about $s = 0.6$ amu$^{1/2}$ bohr and the distance N−H elongates linearly after about $s = -0.2$ amu$^{1/2}$ bohr. This means that the region $-0.2 < s < 0.6$ represents the mainly interacting region of the reaction process. Within this region, whose center position ($s = 0.2$) deviates apparently from the transition state ($s = 0.0$), the H−N bond will be broken and the H−H bond will be formed.

To shed light on the vibrational properties of this reaction, vibrational frequency analyses along the IRC were carried out. The changes of the vibrational frequencies for modes 2−4 are shown in Figure 3. Modes 2 and 3 are two degenerate bending vibrations, and their frequencies only appear in the course of reaction and arrive to a maximum value, 1084 cm^{-1}, at about $s = 0.24$ amu$^{1/2}$ bohr. Mode 4 is a bond-stretching vibrational motion. It can be seen that the frequency of mode 4 changes along the IRC via a deep valley, which has a minimum frequency, 1459 cm^{-1}, at about $s = 0.08$ amu$^{1/2}$ bohr. The depth of this frequency valley is about 2000 cm^{-1} and its width is about from $s = -0.3$ to 0.5 amu$^{1/2}$ bohr. The curve of the frequency of mode 4 links the frequency of NH, 3392 cm^{-1}, at the negative side of s and the frequency of H_2, 4534 cm^{-1}, at the positive side of s. Therefore, mode 4 represents mainly the "key vibration mode" of the abstraction process of hydrogen atom.

As the reaction proceeds, there must be a "critical point" for the vibration transformation from the NH stretching vibration

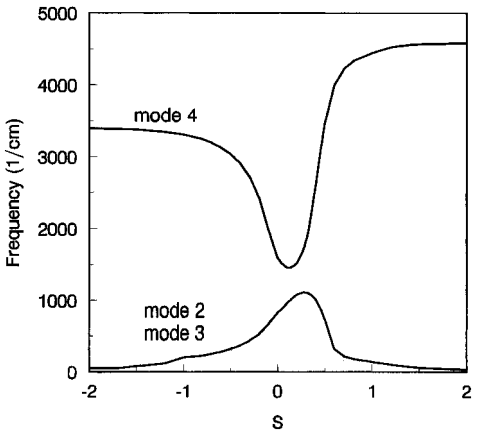

Figure 3. Changes of vibrational frequencies along the IRC as a function of s amu$^{1/2}$ bohr.

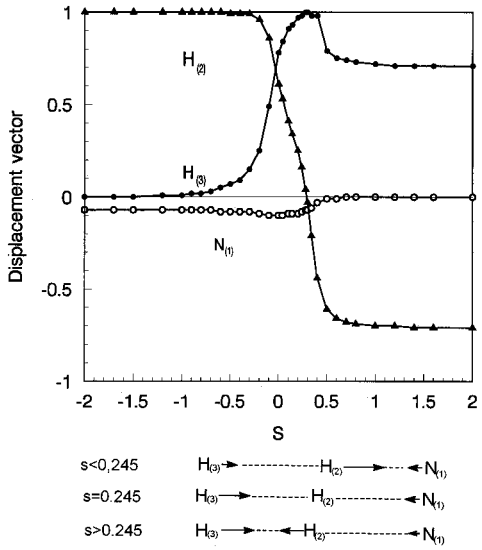

Figure 4. Changes of displacement vectors of atoms in mode 4 along the IRC as a function of s amu$^{1/2}$ bohr.

to the H_2 stretching vibration. To locate the "critical point", the vibrational vector change of each atom of mode 4 along the IRC is drawn in Figure 4. From this figure, we can find that the displacement vector of the harmonic vibration of each atom changes apparently near the point of $s = 0.245$ amu$^{1/2}$ bohr and the displacement vector of the atom $H_{(2)}$ abstracted from NH to H_2 becomes zero at $s = 0.245$ amu$^{1/2}$ bohr. Before this point, the direction of the displacement vector of the atom $H_{(2)}$ is opposite the direction of the displacement vector of the atom $N_{(1)}$ and identical with the direction of the displacement vector of the atom $H_{(3)}$. Thus, there exists only a stretching motion between the atom $N_{(1)}$ and the atom $H_{(2)}$. However, after this point the direction of the displacement vector of the atom $H_{(2)}$ is opposite the direction of the displacement vector of the atom $H_{(3)}$ and identical with the direction of the displacement vector of the atom $N_{(1)}$. This means that the stretching motion of $N_{(1)}-H_{(2)}$ disappears and the stretching motion of $H_{(2)}-H_{(3)}$ appears. Therefore, it can be recognized that the inverted point, at $s = 0.245$ amu$^{1/2}$ bohr, of the direction of the displacement vector of the atom $H_{(2)}$ seems to be a demarcation in the course of the reaction, which divides exactly the reactant side from the product side. This shows that, to reach the products, the reaction needs not only to overcome the reaction potential barrier but also to pass through the inverted point of the displacement vector direction of the atom $H_{(2)}$. This point is referred to as the "critical inversion point" of the key vibration mode. It is probably another factor controlling the progress of reaction.

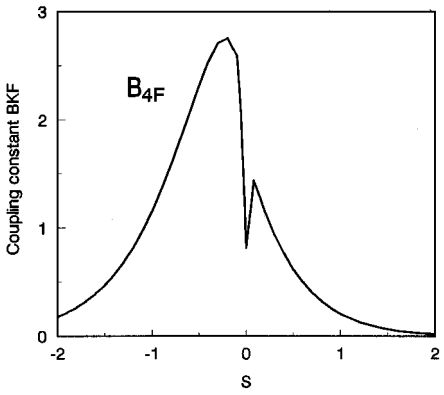

Figure 5. Changes of coupling constants (B_{kF}) along the IRC as a function of s amu$^{1/2}$ bohr.

The coupling constants (B_{KF}) between the IRC and the vibration modes orthogonal to IRC are given in Figure 5. It reveals that there exists only the coupling of the IRC with mode 4, and the others are equal to zero. This means that mode 4 is indeed a key vibration mode of the reaction. Because the maximum of B_{4F} is before $s = 0$, the excitation of this vibration mode would favor the reaction.

C. Rate Constant Calculation. The reaction rate constants for the temperature range 2000−3000 K were obtained using the reaction-path Hamiltonian parameters, the potential energy along the IRC, the first and second energy derivatives, etc. Table 4 lists the results calculated at the UMP2/6-311G**, UQCISD-(T)/6-311G**, and MP-SAC4/6-311G** levels of theory. From

TABLE 4: Reaction Rate Constants, k(10^{13} cm^3 mol^{-1} s^{-1}), for Temperature Range 2000−3000

T (K)	2000	2200	2300	2400	2500	2600	2700	2800	3000
				UMP2(FULL)/6-311G**					
$k^{\ddagger}$	0.890	1.136	1.270	1.410	1.557	1.711	1.872	2.038	2.391
k^{CVT}	0.774	0.982	1.094	1.211	1.333	1.461	1.593	1.728	1.873
$k^{CVT/MEPSAG}$	0.794	1.003	1.116	1.233	1.356	1.483	1.615	1.751	1.894
$k^{CVT/SCSAG}$	0.828	1.038	1.151	1.270	1.393	1.520	1.653	1.789	1.930
				UQCISD(T)/6-311G**					
$k^{\ddagger}$	2.056	2.431	2.628	2.832	3.041	3.257	3.478	3.075	4.175
k^{CVT}	1.788	2.101	2.265	2.433	2.605	2.781	2.960	3.142	3.272
$k^{CVT/MEPSAG}$	1.832	2.144	2.307	2.475	2.646	2.831	3.000	3.182	3.307
$k^{CVT/SCSAG}$	1.872	2.183	2.345	2.512	2.683	2.858	3.036	3.217	3.340
				MP-SAC4/6-311G**					
$k^{\ddagger}$	2.206	2.592	2.795	3.003	3.218	3.439	3.665	3.896	4.377
k^{CVT}	1.928	2.241	2.408	2.581	2.756	2.936	3.119	3.305	3.429
$k^{CVT/MEPSAG}$	1.963	2.284	2.451	2.622	2.797	2.976	3.159	3.344	3.465
$k^{CVT/SCSAG}$	1.997	2.317	2.483	2.654	2.829	3.007	3.189	3.374	3.492
expt[5]	2.949	2.971	2.980	2.989	2.997	3.005	3.012	3.018	3.030

TABLE 5: Reaction Rate Constants, k (cm^3 mol^{-1} s^{-1}), for Temperature Range 300−1800 K at UMP-SAC4 Level

T (K)	300	500	700	900	1200	1400	1600	1800
$k^{\ddagger}$	7.81×10^{11}	2.24×10^{12}	3.92×10^{12}	5.87×10^{12}	9.37×10^{12}	1.21×10^{13}	1.51×10^{13}	1.84×10^{13}
k^{CVT}	7.81×10^{11}	2.23×10^{12}	3.66×10^{12}	5.34×10^{12}	8.38×10^{12}	1.07×10^{13}	1.33×10^{13}	1.61×10^{13}
$k^{CVT/MEPSAG}$	1.98×10^{12}	3.18×10^{12}	4.40×10^{12}	5.98×10^{12}	8.94×10^{12}	1.12×10^{13}	1.38×10^{13}	1.66×10^{13}
$k^{CVT/SCSAG}$	3.11×10^{12}	3.97×10^{12}	4.99×10^{12}	6.47×10^{12}	9.36×10^{12}	1.16×10^{13}	1.42×10^{13}	1.69×10^{13}

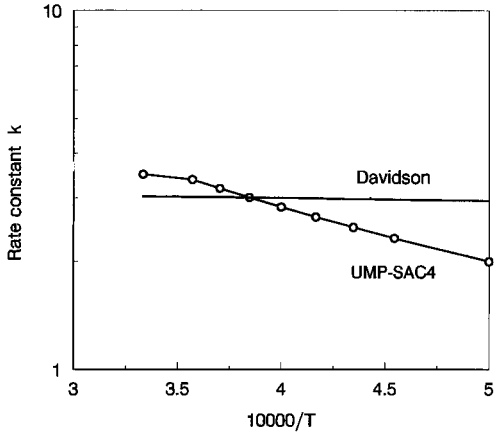

Figure 6. Arrhenius plot of rate constants k (10^{13} cm^{-1} mol^{-1} s^{-1}) vs $1/T$ (K).

TABLE 6: Bottleneck Properties of Reaction (Based on CVT Method)

				bond frequencies (cm^{-1})		
T (K)	s	V_{MEP} (kcal/mol)	V_a^G (kcal/mol)	ω_2	ω_3	ω_4
	0	1.88	6.51	824	824	1592
2000	0.080	1.65	6.41	936	936	1458
2200	0.082	1.63	6.40	938	938	1457
2300	0.083	1.62	6.39	939	939	1457
2400	0.084	1.61	6.38	940	940	1457
2500	0.085	1.60	6.37	941	941	1456
2600	0.086	1.59	6.36	943	943	1456
2700	0.087	1.57	6.35	944	944	1456
2800	0.088	1.55	6.34	945	945	1456
3000	0.127	0.94	5.81	990	990	1467

this table, we can find that the reaction rate constants at the MP-SAC4 and UQCISD(T) levels are in good agreement with the experimental values.[5] A plot of rate constants from the CVT/SCSAG and the experiment is shown in Figure 6. Comparing k^{CVT} with $k^{CVT/MEPSAG}$ and $k^{CVT/SCSAG}$, we can also find that the tunneling and curvature effects are less important for the high-temperature reaction.

In addition, the data in Table 4 show that the rate constants from conventional transition-state theory (‡) are slightly greater than those from variational transition-state theory (CVT). The reason is the bottleneck property of the reaction. The optimal dividing surface corresponds to a minimum rate constant and need not be located at transition state ($s = 0.0$), as seen in Table 6. It can be seen that the location of variational transition state ranges from $s = 0.080$ $amu^{1/2}$ bohr at 2000 K to $s = 0.127$ $amu^{1/2}$ bohr at 3000 K. The potential barrier (V_{MEP}) decreases from 1.88 kcal/mol at $s = 0.0$ to 1.65 kcal/mol at $s = 0.080$ $amu^{1/2}$ bohr and to 0.94 kcal/mol at $s = 0.127$ $amu^{1/2}$ bohr. This illustrates that both the potential energy and vibrational energy play roles in determining the location of the variational transition state.

To explore the tunneling and curvature effects at low temperature, the rate constants at the MP-SAC4 level of theory are calculated for the temperature range 300−1800 K and listed in Table 5. This result shows that the effects of the tunneling and curvature strongly affect the rate constants only around the temperature 300 K.

Conclusion

(1) The potential barrier and the heat of reaction for the hydrogen abstraction reaction, $NH(X^3\Sigma^-) + H \rightarrow N(^4S) + H_2$, are calculated respectively to be 1.68 and −28.95 kcal/mol at the MP-SAC4 level of theory.

(2) By analyzing the geometrical change of the reaction along the IRC, we have found that the reaction region of the bond breaking and the bond forming is about $s = -0.2$ to 0.6 $amu^{1/2}$ bohr.

(3) The changes of the frequencies and the displacement vectors along the IRC show that mode 4 plays an important role in the course of this reaction. Also, the "critical inversion point", $s = 0.245$ $amu^{1/2}$ bohr, of the displacement vector direction of the atom $H_{(2)}$ in mode 4 is a demarcation dividing the reactant side from the product side.

(4) The calculated rate constants based on the UQCISD(T) and MP-SAC4 levels of theory agree well with the experimental ones in the temperature range 2000−3000 K. The tunneling and curvature effects are less important for the high-temperature reactions.

Acknowledgment. The project was supported by the National Natural Science Foundation of China (NNSFC).

References and Notes

(1) Dove, J. E.; Nip, W. S. *Can. J. Chem.* **1979**, *57*, 689.

(2) Davidson, D. F.; Kohse-Hoingaus, K.; Chang, A. Y.; Hanson, R. K. *Int. J. Chem. Kinet.* **1990**, *22*, 513.

(3) Miller, J. A.; Bowman, C. T. *Prog. Energy Combust. Sci.* **1989**, *15*, 287.

(4) Morly, C. *18th Symposium (International) on Combustion*; The Combustion Institute: Pittsburgh, 1981; p 23.

(5) Davidson, D. F.; Hanson, R. K. *Int. J. Chem. Kinet.* **1990**, *22*, 843.

(6) Mayer, S. W.; Schieler, L. *J. Phys. Chem.* **1968**, *72*, 236.

(7) Johnston, H. S.; Parr, C. *J. Am. Chem. S0c.* **1963,** *85*, 2544.

(8) Truhlar, D. G.; Garrett, B. C. *Acc. Chem. Res* **1980**, *13*, 440.

(9) Truhlar, D. G.; Isaacson, A. D.; Garrett, B. C. In *Theory of Chemical Reaction Dynamics*; Baer, M., Ed.; CRC Press: Boca Raton, FL, 1985; p 65.

(10) Baldridge, K. M.; Gordon, M. S.; Steckler, R.; Truhlar, D. G. *J. Phys. Chem.* **1989**, *93*, 5107.

(11) Garrett, B. C.; Truhlar, D. G.; Grev, R. S.; Magnuson, A. W. *J. Phys. Chem.* **1980**, *84*, 1730.

(12) Xu, Z.-F.; Fang, D.-C.; Fu, X.-Y. *J. Phys. Chem.* **1995**, *16*, 5889.

(13) Fukui, K. *J. Phys. Chem.* **1970**, *74*, 4161.

(14) Miller, W. H. In *Potential Energy Surface and Dynamics Calculations*; Truhlar, D. G., Ed.; Plenm Press: New York, 1981; p 265.

(15) Frisch, M. J.; Trucks, G. W.; Head-Gordon, M.; Gill, P. M. W.; Wong, M. W.; Foresman, J. B.; Johnson, B. G.; Schlegel, H. B.; Robb, M. A.; Replogle, E. S.; Gomperts, R.; Andres, J. L.; Raghavachari, K.; Binkley, J. S.; Gonzalez, C.; Martin, R. L.; Fox, D. J.; Defrees, D. J.; Stewart, J. J. P.; Pople, J. A. *Gaussian 92*; Gaussian, Inc.; Pittsburgh, PA, 1992.

(16) Hehre, W. J.; Radom, L.; Schleyer, P. V. R.; Pople, J. A. *Ab Initio Molecular Orbital Theory*; Wiley: New York, 1986.

(17) Pople, J. A.; Binkley, J. S.; Seeger, R. *Int. J. Quantum Chem. Symp.* **1976**, *10*, 1.

(18) Pople, J. A.; Head-Gordon, M.; Raghavachari, K. *J. Chem. Phys.* **1987**, *87*, 5968.

(19) Gordon, M. S.; Truhlar, D. G. *J. Am. Chem. Soc.* **1986**, *108*, 5412.

(20) Isaacson, A. D.; Truhlar, D. G.; Rai, S. N.; Steckler, R.; Hancock, G. C. *POLYRATE*; University of Minnesota, MN, 1987.

(21) Huber, K. P.; Herzberg, G. *Molecular Spectra and Molecular Structure (IV). Constants of Diatomic Molecules*; Van Nostrand Reinhold: New York, 1979.